Nucleic Acids Research, 2005, Vol. 33, No. 14 ***4649–4659***
doi:10.1093/nar/gki782

Not so crystal clear: the structure of the human telomere G-quadruplex in solution differs from that present in a crystal

Jing Li, John J. Correia, Lei Wang[1], John O. Trent[1] and Jonathan B. Chaires[1,*]

Department of Biochemistry, University of Mississippi Medical Center, 2500 North State Street, Jackson, MS 39216-4505, USA and [1]James Graham Brown Cancer Center, University of Louisville, 529 South Jackson Street, Louisville, KY 40202, USA

Received July 22, 2005; Revised and Accepted August 4, 2005

ABSTRACT

The structure of human telomere DNA is of intense interest because of its role in the biology of both cancer and aging. The sequence [5′-AGGG(TTAGGG)$_3$] has been used as a model for telomere DNA in both NMR and X-ray crystallographic studies, the results of which show dramatically different structures. In Na^+ solution, NMR revealed an antiparallel G-quadruplex structure that featured both diagonal and lateral TTA loops. Crystallographic studies in the presence of K^+ revealed a flattened, propeller-shaped structure featuring a parallel-stranded G-quadruplex with symmetrical external TTA loops. We report the results of biophysical experiments in solution and computational studies that are inconsistent with the reported crystal structure, indicating that a different structure exists in K^+ solutions. Sedimentation coefficients were determined experimentally in both Na^+ and K^+ solutions and were compared with values calculated using bead models for the reported NMR and crystal structures. Although the solution NMR structure accurately predicted the observed *S*-value in Na^+ solution, the crystal structure predicted an S-value that differed dramatically from that experimentally observed in K^+ solution. The environments of loop adenines were probed by quantitative fluorescence studies using strategic and systematic single-substitutions of 2-aminopurine for adenine bases. Both fluorescence intensity and quenching experiments in K^+ yielded results at odds with quantitative predictions from the reported crystal structure. Circular dichroism and fluorescence quenching studies in the presence of the crowding agent polyethylene glycol showed dramatic changes in the quadruplex structure in K^+ solutions, but not in Na^+ solutions, suggesting that the crystal environment may have selected for a particular conformational form. Molecular dynamics simulations were performed to yield model structures for the K^+ quadruplex form that are consistent with our biophysical results and with previously reported chemical modification studies. These models suggest that the biologically relevant structure of the human telomere quadruplex in K^+ solution is not the one determined in the published crystalline state.

INTRODUCTION

Human telomere DNA consists of 5–8 kb of tandem repeats of the sequence d(TTAGGG), with a single-stranded 3′ overhang of 100–200 nt (1). In solution, the G-rich overhang can fold into G-quadruplex structures that consist of stacked G-quartets, a square planar arrangement of four guanines stabilized by an array of Hoogsten hydrogen bonds (2). The exact structure and function of these G-quadruplexes is of intense current interest because of their relevance to the biology of cancer (3–5), aging (6,7) and genetic recombination (8,9). G-quadruplexes of different sequences are also found in promoter regions that control gene expression (10–14). G-quadruplexes are an attractive target for drug design, especially for cancer chemotherapy (3–5,15–18) and for modulation of transcription (19–21). For structure-based drug design strategies to succeed, accurate structures for the human telomere quadruplex under biologically relevant conditions must be available.

The 22 nt sequence d[AGGG(TTAGGG)$_3$] has been used as a model for the G-quadruplex structure within the single-strand overhang in human telomeres. Wang and Patel (22) solved the Na^+ solution structure of that sequence by NMR. They found that the sequence folds intramolecularly into an antiparallel stranded structure containing three stacked

*To whom correspondence should be addressed. Tel: +1 502 852 1172; Fax: +1 502 852 1153; Email: j.chaires@louisville.edu

G-quartets, with a diagonal d(TTA) loop at one end and two lateral d(TTA) loops at the other end (Figure 1a). Parkinson *et al*. (23) subsequently reported a radically different structure of the same sequence in K^+ determined by crystallography. They found that the 22 nt sequence folded into a parallel-stranded intramolecular quadruplex containing three G-quartets, and three symmetrical external d(TTA) loops positioned in a propeller-like arrangement along the sides of the quadruplex core (Figure 1b). Our laboratory created an object dubbed 'tiny telomere' DNA in which the human telomere quadruplex structure was linked to a 12 bp DNA duplex, providing a model for the junction region between the folded quadruplex and duplex regions (24).

The crystal structure of the human telomere quadruplex ('ht-quadruplex') has been used as a basis for structure-based drug design (18,25). However, several solution studies reported results that are inconsistent with specific features of the crystal structure. In studies that predated the crystal structure, the structure and stability of the human telomere repeat sequence was studied in both Na^+ and K^+ solutions by circular dichroism and chemical modification studies (26). Dramatic differences in circular dichroism spectra were found between Na^+ and K^+ solutions. The pattern of reactivity of adenine residues toward diethyl pyrocarbonate (DEPC), however, was similar in both Na^+ and K^+, suggesting that there was no radical rearrangement of the d(TTA) loop structures. Chemical cross-linking studies using platinum compounds showed similar patterns of reactivity in Na^+ and K^+ solutions (27). The base proximity relationships inferred from the cross-linking studies were inconsistent with the specific features of the quadruplex observed in the crystal. It was recently concluded from single molecule FRET studies on ht-quadruplex structures linked to a duplex that the antiparallel conformation was the dominant conformation in both Na^+ and K^+ solutions (28). Radioprobing experiments with ^{125}I were recently reported, suggesting that an antiparallel quadruplex conformation existed in both Na^+ and K^+, contrary to the specific features of the crystal structure (29). Finally, from the results of chemical ligation studies in solution, Qi and Shafer (30) concluded that the circular product was derived from an antiparallel quadruplex form rather than from a parallel structure regardless of ion type for the ions K^+, Na^+, Pb^{2+} and Ba^{2+}. It is not uncommon for quadruplex structures obtained by crystallography to disagree with those obtained in solution (31). Quadruplex structures appear to be both labile and mobile, with numerous conformational states available. The crowded, dehydrating conditions necessary for crystallization perhaps represent an artificial environment that might well select for particular conformations that are not predominant in solution. In order to explore the biologically relevant conformation of ht-quadruplex in solution, we used a battery of proven biophysical techniques coupled with molecular dynamics simulations.

Analytical ultracentrifugation is a thermodynamically rigorous approach for the determination of absolute molecular weights and for obtaining quantitative information about the hydrodynamic shapes of macromolecules in solution (32,33). Recently, it has become possible to calculate the hydrodynamic properties of macromolecules from their known atomic level structures by the use of 'bead' models (34–36). These models make it possible to link empirical or theoretical structures with hydrodynamic measurements in solution. Here, we report experimentally determined molecular weights and sedimentation coefficients for the ht-quadruplex in Na^+ and K^+ solutions, and compare these with values calculated from reported high-resolution structures.

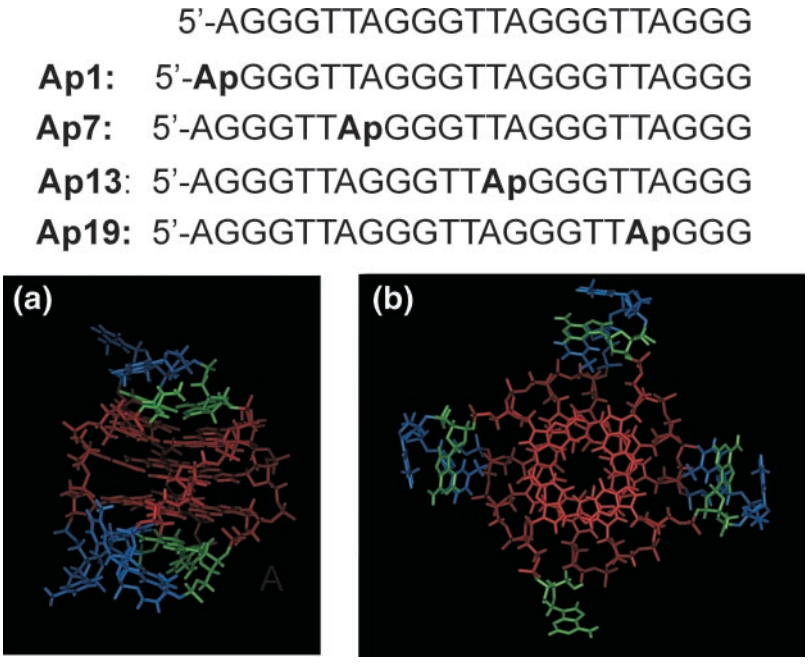

Figure 1. Sequences and structures of human telomere DNA. The sequences used in this study are shown at the top. The unmodified 22 nt sequence is listed first. Singly substituted oligonucleotides containing 2-aminopurine ('Ap') are shown with the position of the substitution in bold. (**a**) NMR-derived structure of the human telomere DNA sequence in Na^+ reported by Wang and Patel (22). (**b**) Structure of human telomere DNA in Na^+ derived from crystallographic studies reported by Parkinson *et al*. (23).

The modified base 2-aminopurine (2-AP) has been used for >30 years as a fluorescent probe for nucleic acids (37–40). The quantum yield of 2-AP is very sensitive to its environment, and 2-AP fluorescence is quenched when it is stacked with other bases. 2-AP behaves like adenine and forms a base pair with thymine. Substitution of 2-AP for adenine has little effect on duplex DNA structure or stability. We report the use of 2-AP to probe the loop environments of the ht-quadruplex in Na^+ and K^+ solutions. Systematic single-substitutions were made (Figure 1) to replace each of the four adenines with 2-AP. Fluorescence emission intensity and fluorescence quenching (41) studies provide quantitative measures of the environment of loop adenines that can be compared with the properties of these residues in reported high-resolution structures.

The results of our biophysical studies are fully consistent with the antiparallel structure in Na^+ solutions that was described by Wang and Patel (22). However, both sedimentation and fluorescence experiments in K^+ solutions yield results that are inconsistent with the reported crystal structure (23). Based on these studies, the crystal structure cannot be the predominant structure that exists in solution.

METHODS

Preparation of DNA

The DNA oligonucleotide d[AGGG(TTAGGG)$_3$] and its fluorescent analogs (Figure 1) were purchased from Oligos Etc. (http://www.oligosetc.com) and were used without further purification. A molar extinction coefficient of 196 479 ± 5675 M^{-1} cm^{-1} at 260 nm at 20°C was determined for the folded quadruplex form by means of a colorimetric phosphate assay (42). Oligonucleotides were digested with P1 nuclease and alkaline phosphatase (Sigma–Aldrich) in NP1 buffer (NaAc 30 mM and $ZnCl_2$ 1 mM, pH 6.5) for both extinction coefficient determination and for fluorescence control experiments. BPES and BPEK buffers (consisting of 6 mM Na_2HPO_4, 2 mM NaH_2PO4, 1 mM Na_2EDTA, 185 mM NaCl or KCl, pH 7.1) were used for all experiments.

Steady-state fluorescence spectra and quenching experiments

Steady-state fluorescence measurements were carried out with a JASCO model FP-6500 flurometer equipped with a Peltier temperature controller. Oligonucleotides were excited at 305 nm with slit width of 5 nm, and emission spectra were collected from 320–420 nm. For the acrylamide quenching experiments, aliquots of a 4 M acrylamide stock solution were added to oligonucleotide solutions to bring the final concentration into the range of 0–0.7 M, using an excitation wavelength of 305 nm and an emission wavelength of 370 nm.

Circular dichroism spectra

Circular dichroism experiments were performed on a JASCO model J-810 circular dichroism spectrapolarimeter equipped with a Peltier temperature controller.

Sedimentation equilibrium and velocity experiments

Sedimentation experiments were performed using a Beckman Optima XLA analytical ultracentrifuge equipped with absorbance optics and an An60Ti rotor. Sedimentation velocity experiments were performed at 20°C using a rotor speed of 50 000 r.p.m., with three loading concentrations of 0.25, 0.5 and 1 OD at 260 nm. Analysis of sedimentation velocity experiments was performed with the program *Sedfit* (43). Sedimentation equilibrium measurements were performed at 20°C using a rotor speed of 34 000 r.p.m. Three initial sample concentrations of 0.25, 0.5 and 1.0 $OD_{260\ nm}$ were scanned in six channel centerpieces after equilibrium of ~6 h. Sedimentation equilibrium experiments were analyzed using the software package *Sedanal* (44). The best fit of oligonucleotides molecular weight was calculated by Monte Carlo analysis.

Molecular dynamics simulations

The d[AGGG(TTAGGG)$_3$] crystal structure (PDB code 1KF1) and NMR structure (143d) were used directly for molecular dynamics calculations. Two sodium or potassium ions were placed in the experimentally observed positions, between quartet stacks. The chair model was generated to be consistent with the literature (26,45). The all-clockwise quartet structure was generated from the crystal and NMR structure. The models were solvated in a 10 Å box of TIP3P water by using standard Amber 8.0 rules to hydrate the systems and counter-ions were added randomly for overall charge neutrality. Periodic boundary conditions and the particle mesh Ewald algorithm were used. A 2.0 fs time-step was used with bonds involving hydrogen frozen using SHAKE. Molecular dynamics (MD) calculations were carried out with the AMBER 8.0 mpi version of sander and parm98.dat parameterization. Simulations were performed in the isothermic isobaric ensemble (P 1 atm; T 300 K). The systems were heated slowly and equilibrated for 125 ps with gradual removal of positional restraints on the DNA following this protocol: (i) minimize water, (ii) 25 ps MD (T 100 K) holding DNA fixed (100 kcal/mol $Å^{-1}$), (iii) minimize water; (iv) minimize total system, (v) 25 ps MD (T 100 K) holding DNA fixed (100 kcal/mol $Å^{-1}$), (vi) 25 ps MD (T 300 K) holding DNA fixed (100 kcal/mol $Å^{-1}$), (vii) 25 ps MD (T 300 K) holding DNA fixed (50 kcal/mol $Å^{-1}$), (viii) 25 ps MD (T 300 K) holding DNA fixed (10 kcal/mol $Å^{-1}$) and (ix) 25 ps MD (T 300 K) holding DNA fixed (1 kcal/mol $Å^{-1}$). Production runs of 4 ns after final equilibrium were used to obtain snapshots at 2 ps throughout the trajectory and average structures, (25 snapshots in the last 50 ps), which were subsequently minimized (1000 steps steepest descents followed by 5000 steps conjugate gradient) using GB/SA solvation and the AMBER* force field in Macromodel (46). Perl scripts was generated to calculate the sedimentation coefficient using HYDROPRO 5a[35] and to calculate the solvent accessible surfaces using NACCESS 2.1.1 (47) for the last 2 ns of each trajectory. Calculations were performed on Silicon Graphics Origin 2000 server.

RESULTS

Measured sedimentation coefficients are consistent with NMR results in Na^+, but not with crystallographic studies in K^+

Sedimentation velocity and sedimentation equilibrium experiments were performed to characterize the hydrodynamic

Table 1. Sedimentation properties of G-quadruplexes in Na^+ and K^+ solutions

Parameter	Units	Na^+ Form	K^+ Form
$S_{exp}/10^{-13a}$	s	1.92 ± 0.01	2.11 ± 0.01
$S_{calc}/10^{-13b}$	s	1.86 ± 0.02	1.69 ± 0.02
$D_{exp}/10^{-6c}$	$cm^2\ s^{-1}$	1.49 ± 0.04	1.62 ± 0.02
$D_{calc}/10^{-6b}$	$cm^2\ s^{-1}$	1.40 ± 0.01	1.32 ± 0.02
Molecular weight[d]	Da	7041 ± 158	7119 ± 57
Calculated MW	Da	7107.4	7107.4

[a]Determined by sedimentation velocity experiments. Corrected to standard conditions of water, 20°C.
[b]Calculated using HYDROPRO.
[c]Calculated from S and MW. The error is estimated by propagation of the errors in S and M.
[d]Determined by sedimentation equilibrium experiments.

properties of the ht-quadruplex in Na^+ and K^+ solutions. Both techniques show that under either salt condition the ht-quadruplex is monomeric, with no >2% of the population present as higher molecular weight species. The results of sedimentation experiments are presented in Table 1. Sedimentation coefficients (S) and molecular weights (MW) were measured directly by experiment, and diffusion coefficients were calculated from S and MW values. Molecular weights obtained by sedimentation equilibrium differ by no >1% from molecular weights calculated from the known sequence of the oligonucleotide used in these studies.

Figure 2 shows the results of sedimentation velocity experiments in Na^+ and K^+. Data were analyzed using the c(s) method (43) to provide high-resolution sedimentation coefficient distributions. *S*-values were found to be independent of the loading concentration. In Na^+, S = 1.92 ± 0.01 was measured. A higher value, S = 2.11 ± 0.01 was found in K^+ solutions. The 9.9% increase in S is statistically significant, indicating that a hydrodynamically more compact conformation exists in K^+ relative to Na^+ solutions. Diffusion coefficients calculated from S and M values (Table 1) are also consistent with a transition to a hydrodynamically more compact shape in K^+ solutions.

The hydrodynamic properties of macromolecules may be calculated from known atomic-level structures by using 'bead' models (35,36). Examples of bead models calculated for the Na^+ and K^+ quadruplex forms from their reported high-resolution structures are shown in Supplementary Figure 1. Distributions of calculated sedimentation coefficients for the Na^+ and K^+ ht-quadruplex forms are shown in Figure 2. The results show striking differences between calculated and actual *S*-values for the K^+ form, but not the Na^+ form.

The NMR determined structure of the Na^+ form of the ht-quadruplex yields calculated hydrodynamic properties that are in excellent agreement with experimentally determined values (Table 1). An *S*-value of 1.86 ± 0.02 is calculated from the structure, a value that is within 3.2% of the experimentally determined value of 1.92 ± 0.01. The NMR structure accurately predicts the experimental hydrodynamic properties of the ht-quadruplex in Na^+ solutions.

In sharp contrast, the crystal structure of the K^+ form of the ht-quadruplex fails to predict the experimentally observed hydrodynamic properties. The calculated *S*-value was found to be 1.69 ± 0.02, a value 24.9% lower than the experimentally observed $S = 2.11 \pm 0.01$ (Table 1). The difference between the calculated and observed *S*-value is well beyond

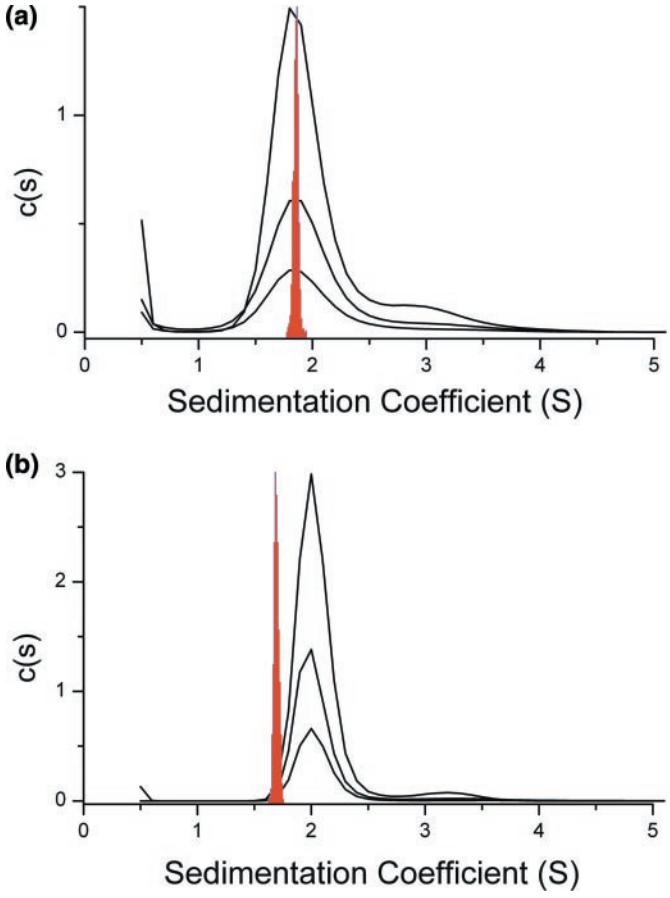

Figure 2. Results from sedimentation velocity experiments and molecular dynamic simulations. Sedimentation coefficient distributions as determined by the program *Sedfit* (43) are shown for Na^+ solutions (**a**) or K^+ solutions (**b**), yielding the values shown in Table 1. Data for three different loading concentrations are shown (5.1, 2.55 and 1.275 μM strand). The narrower distributions in red were calculated from molecular dynamics trajectories for simulations based on the Wang–Patel (22) structure (a) or the Parkinson–Lee–Neidle structure (23) (b).

the experimental error of the measurement or of the distribution of values calculated from the molecular dynamics ensemble. As shown in Figure 2b, the calculated sedimentation coefficient distribution differs significantly from the experimental *S*-value distribution. The reported crystal structure does not account for the hydrodynamic properties of the ht-quadruplex in solution, suggesting that a different conformation exists in solution. The conformation in K^+ solution must be hydrodynamically more compact than the one observed in the crystal.

Fluorescence studies using samples strategically substituted with 2-AP yield results that are inconsistent with predictions derived from the structure of the K^+ ht-quadruplex in the crystal

The ht-quadruplex was strategically substituted with 2-AP at specific adenine residues in order to provide a fluorescence probe with which to investigate loop environments. The substitutions are shown in Figure 1. Control experiments (Supplementary Figure 2) established that substitution of

specific adenines by 2-AP does not alter the global structure of the ht-quadruplex in either Na^+ or K^+ as judged by circular dichroism spectroscopy, nor does it appreciably alter the thermal stability of the structures, as judged by thermal denaturation studies.

Figure 3 shows the steady-state fluorescence properties of 2-AP-substituted quadruplex structures. In Na^+ solutions (Figure 3a), the fluorescence emission intensity differs for each of the substitutions. 2-AP fluorescence is most quenched for the A-13 position and least quenched when at the A-7 position. Intermediate quenching is seen for the A-1 and A-19 positions. In the NMR structure reported by Wang and Patel (22), A-1, A-13 and A-19 were all reported to be stacked upon G-tetrads, while only A-7 was unstacked and tilted relative to the tetrad plane. The pattern of fluorescence emission intensities in Figure 3a is fully consistent with these structural features. Fluorescence quenching experiments (Figure 3b) were used to probe the accessibility of 2-AP residues, using acrylamide as a collisional quencher. The observed accessibility followed the order (from least to most accessible): A-13 < A-1 < A-7 ≈ A-19. In the Wang–Patel (22) structures, A-13 and A-1 are packed within a diagonal loop at one end of the quadruplex, while A-7 and A-19 are in separate lateral loops at the opposite end. The order of the accessibility is consistent with the adenine environments seen in the structure.

Similar studies in K^+ yield results that are inconsistent with the expectations of the reported crystal structure and which are different from the NMR basket structure. The crystal structure shows that residues A-7, A-13 and A-19 are all in equivalent loop environments, with each intercalated between thymine residues. The terminal A-1 residue is unstacked and is not in a loop. The crystal structure thus predicts only two types of environments, one for A-1, and another for the symmetrically equivalent A-7, A-13 and A-19 residues. In contrast to the prediction, a greater diversity of environments is observed in fluorescence studies (Figure 3c and d). The order of fluorescence emission intensities was observed to be A-13 < A-1 = A-19 < A-7. As all of the residues in the crystal structure except A-1 are in identical environments, the intensities of A-7, A-13 and A-19 ought to be identical. The order of accessibility to acrylamide quenching was found to be A-13 < A-19 < A-1 = A-7. This contradicts the expectation that A-7, A-13 and A-19 should be accessible to the same extent. Indeed, from the crystal structure, solvent accessible surface areas (in $Å^2$) for the adenine bases are calculated to be: A-1 = 196.4; A-7 = 98.3; A-13 = 90.9; A-19 = 96.3. The pattern of quenching data in Figure 3d

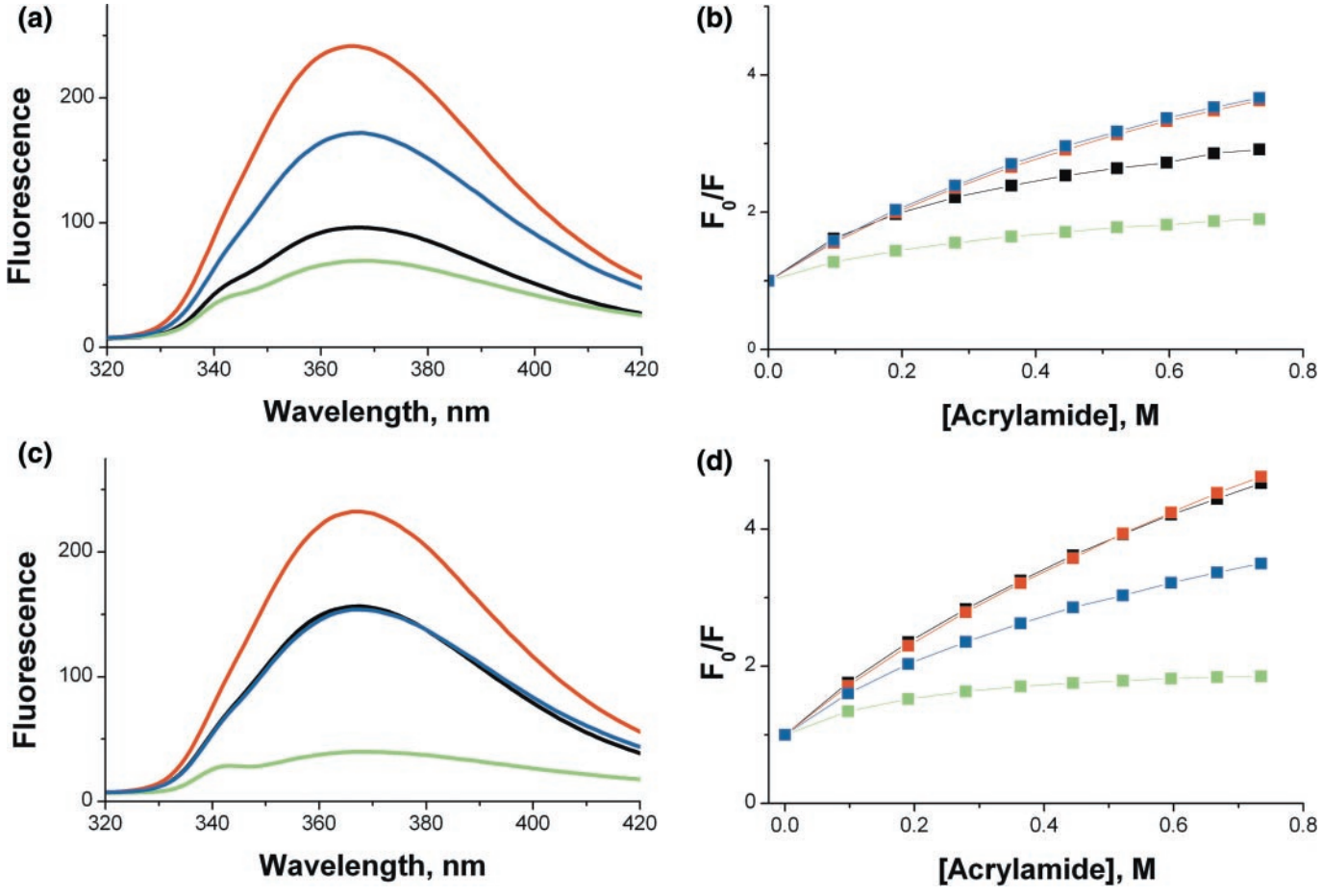

Figure 3. Results of fluorescence studies. The results of fluorescence intensity measurements (**a** and **c**) or fluorescence quenching studies using acrylamide (**b** and **d**) are shown for oligonucleotides containing 2-aminopurine. The top row (a and b) shows results obtained in Na^+, while the bottom row (c and d) shows results obtained in K^+. The colors indicate the position of the 2-aminopurine substitution: **Ap1**, black; **Ap7**, red; **Ap13**, green; **Ap19**, blue.

quantitatively disagrees with calculated solvent accessible surface areas from the crystal structure, suggesting that the structure in solution is distinctly different from that in the crystal.

Some aspects of the fluorescence data deserve additional comment. The curvature seen in acrylamide quenching curves (Figure 3b and d) may be attributed to dynamic heterogeneity of 2-AP residues within quadruplex structures, a reflection of base motions. The fluorescence lifetime of 2-AP is known to shift from a simple monoexponential decay to a multiple exponential decay when substituted into all forms of DNA, a phenomenon attributed to the existence of an ensemble of conformational states for the base (37,39). The curvature in quenching curves is an expected manifestation of such a lifetime distribution.

Supplementary Figure 3 illustrates a control experiment, which shows that upon digestion of substituted quadruplex structures by P1 nuclease (releasing the 2-AP residues) there is a dramatic increase in fluorescence emission intensity. In addition, the accessibility to acrylamide quenching becomes identical for all sequences. This shows that quenching of the intact structures is not due to artifacts, such as inner filter effects arising from acrylamide absorbance.

The fluorescence quenching studies shown in Figure 3 indicate that certain 2-AP residues are more accessible in K^+ than in Na^+. The data are replotted in Supplementary Figure 4 to emphasize these differences. The quenching and accessibility of A-13 and A-19 are virtually identical regardless of the salt, while residues A-1 and A-7 become more accessible in K^+ compared with Na^+.

Crowding alters the structure of the K^+ quadruplex, but not the Na^+ form

Polyethylene glycol (PEG 400) was used to test the effects of crowding on the structure of ht-quadruplexes in Na^+ and K^+. A crowding agent like PEG 400 acts by occupying solution volume, driving reactions to conformations or associated states with the minimal excluded volume. The results are shown in Figure 4. While the global structure (as measured by circular dichroism) of the quadruplex is only slightly altered by the addition of PEG to Na^+ solutions (Figure 4a), more dramatic changes are evident in K^+ solutions (Figure 4c). In K^+, addition of PEG results in the development of a peak near 265 nm, and a clear isoselliptic point at 253 nm. These data suggest a transition between two conformational states in

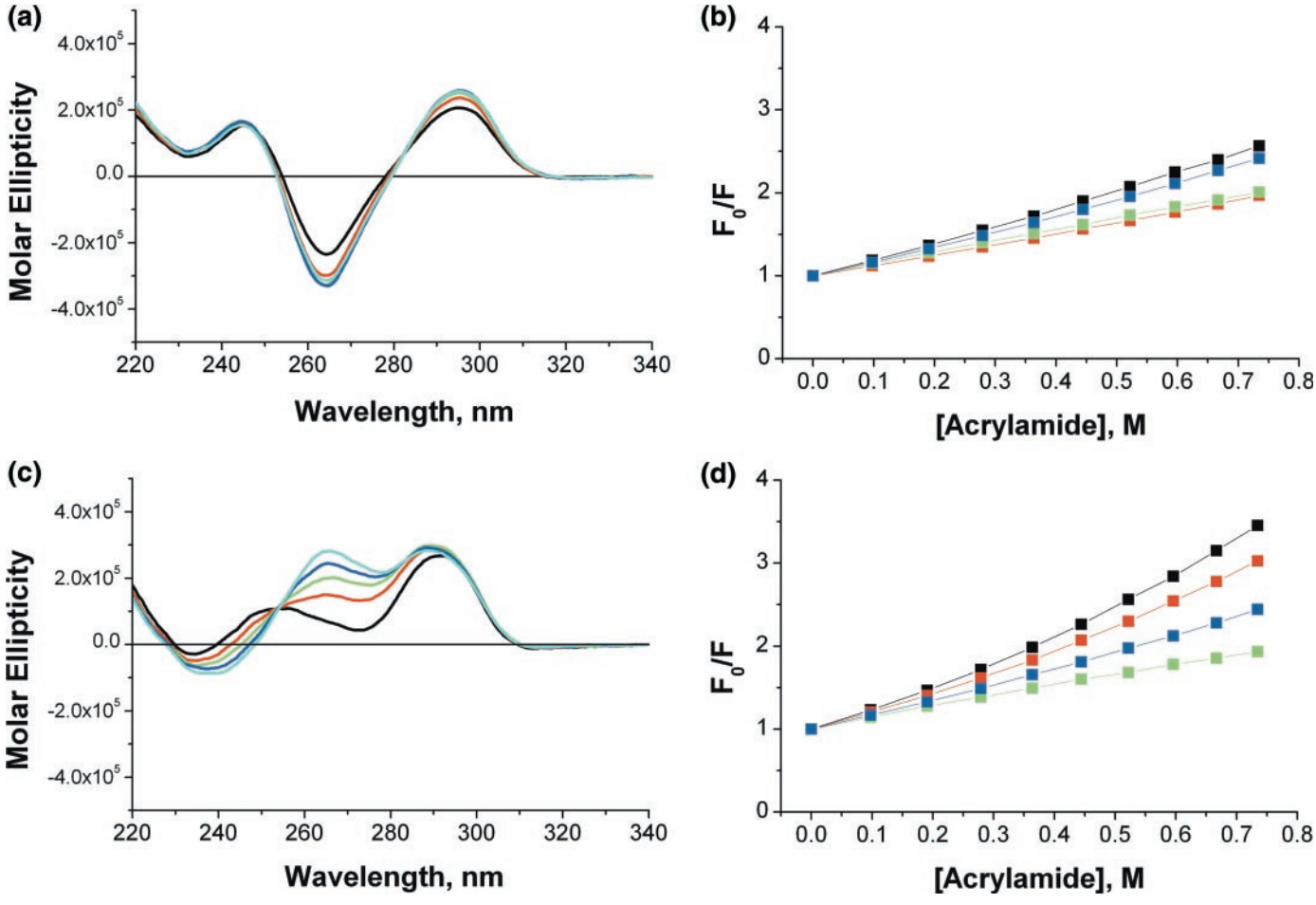

Figure 4. Effect of the crowding agent polyethyleneglycol (PEG) on quadruplex structure. The top row (**a** and **b**) shows results obtained in Na^+. The bottom row shows results obtained in K^+. CD spectra are shown in (a and c), while acrylamide fluorescence quenching curves are shown in (b and d). CD spectra were recorded with no PEG (black curves) to a maximum of 1.4 M PEG (cyan curves). Fluorescence quenching experiments were performed in 1.4 M PEG.

K^+ upon addition of PEG. Addition of PEG affects residue accessibility to acrylamide quenching in both Na^+ and K^+ solutions (Figure 4b and d). These results suggest that crowded environments, such as in the crystalline state, might drive the selection of a particular conformational form.

Sedimentation values of parallel and antiparallel quartet structures

A calculated sedimentation value of 2.08 S was obtained for a model of the antiparallel G-quartet stack alone constructed from the Wang–Patel structure by deleting the 5′-A and the three TTA loop structures. Similarly, a value of 2.24 S was calculated for a parallel three quartet stack model, derived from the crystallographic structure of a parallel quartet, $d(TGGGGT)_4$ (48). The observed experimental value of 2.11 for the K^+ form suggests that there must be little contribution by the loop regions to the hydrodynamic properties, indicating that they must be in a very compact and ordered conformation.

Molecular dynamics calculations on alternative parallel and antiparallel structures

To explore possible alternative structures, molecular models were generated with a variety of strand orientations, loop geometries and quartet orientations. Models that were explored are shown in Figure 5, with their properties described in Table 2. We also found that molecular dynamics simulations of the reported K^+-parallel (22) and Na^+-antiparallel (23) structures were stable, and that their key topological features were maintained over >4 ns trajectories. These structures were used as points of departure to explore other conformations (Table 2 and Figure 5). Three major structural features, in several combinations, were used to generate alternative structures. These features include: (i) loop topology, with either a 'basket' (diagonal loop) or a 'chair' (lateral loop) form; (ii) the direction of the bases within the quartets (clockwise or anticlockwise); and (iii) forms with different topological rotation of the direction of the strands, right- or left-handed defined by the position of the second guanine base forming the G-quartet with respect to the 5′-AGGG position. These structures were all topologically stable in unrestrained molecular dynamics trajectories. The minimized average structures were determined and sedimentation values were subsequently calculated for these structures using HYDROPRO. Results are summarized in Table 2.

None of the seven alternate structures that were considered in detail was able to match exactly the experimentally observed sedimentation coefficient (2.11 S) for the K^+ form. The experimental value is most closely matched by G-quadruplex structures with no loops at all. This indicates that the K^+ form may have a structured, compact loop

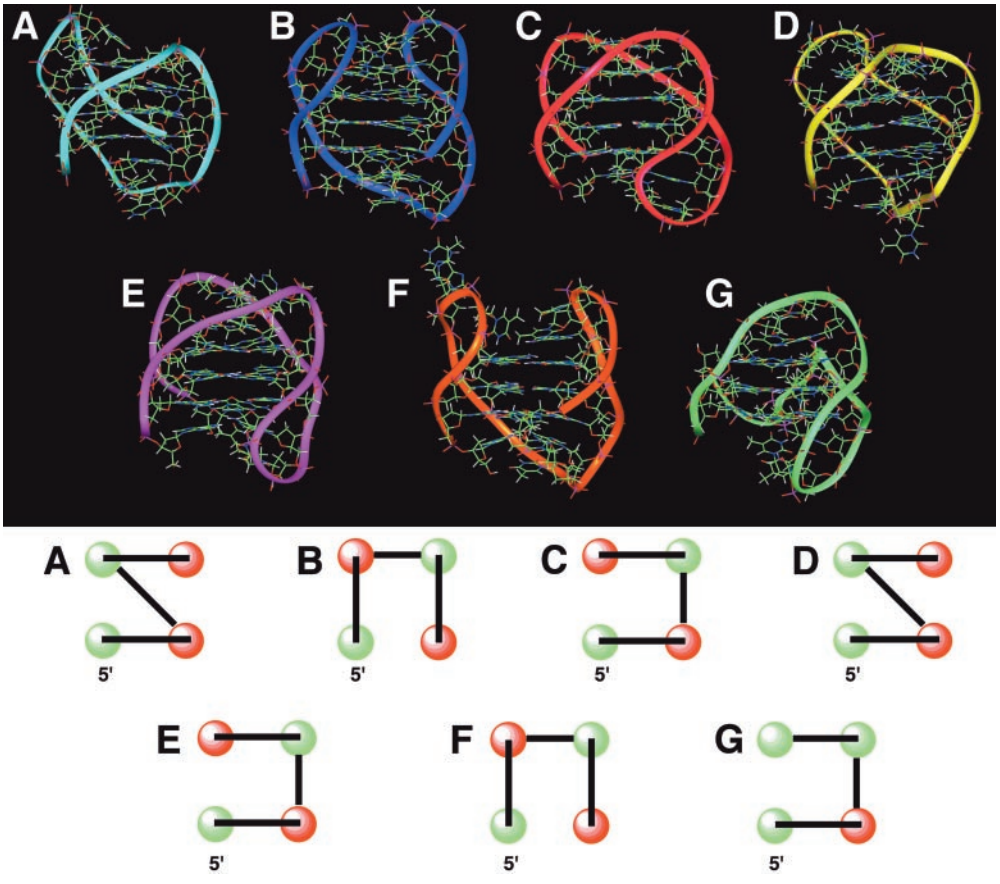

Figure 5. Alternative structures for the human telomere quadruplex in K^+ solutions. Top panel: minimized structures (A–G) built with the properties listed in Table 2. Bottom panel: schematics of the quadruplex structures shown in the top panel as viewed from above are shown. Green circles represent 5′ to 3′ strand direction toward the reader and red circles indicate 5′ to 3′ strand direction pointing away from the reader. The lines representing the loops are topologically correct.

Table 2. Sedimentation values for known and alternative K^+ structures

	Overall fold[a]	Rotation of fold[b]	Quartet rotation[c]	Loop orientation[d]	Energy (kJ/mol)	Sedimentation value[e]
X-ray	Parallel	Right	Clockwise	Propeller	−18 940[f] (−18 914[g])	1.72[f] (1.69[g])
NMR	Antiparallel	Right	Alternating	Basket	−19 279[h] (−19 057[i])	1.92[h] (1.89[i])
A	Antiparallel	Right	Clockwise	Basket	−19 248	1.88
B	Antiparallel	Left	Alternating	Chair	−19 201	1.86
C	Antiparallel	Right	Clockwise	Chair	−19 239	1.86
D	Antiparallel	Right	Anticlockwise	Basket	−19 177	1.86
E	Antiparallel	Right	Alternating	Chair	−19 095	1.83
F	Antiparallel	Left	Clockwise	Chair	−19 119	1.81
G	Antiparallel	Right	Alternating	Mixed	−19 093	1.80

[a]Parallel: the four backbone regions of guanines are in the same 5′ to 3′ direction. Antiparallel: the four backbone regions of guanines are in the different 5′ to 3′ directions.
[b]Topological rotation of the direction of the strands, right- or left-handed defined by the position of the second quanine bases forming the G-quartet with respect to the 5′-AGGG position.
[c]The rotational direction of the bases within the G-quartets. Clockwise has all three quartets with the bases in the same clockwise rotation as in the crystal structure. Anticlockwise has all three quartets with the bases in the same anticlockwise rotation opposite to that in the crystal structure. Alternating has the three quartets in the same rotational orientation as in the NMR structure.
[d]Location of the loops. Propeller: loops running exteriorly to the G-quartets; Basket: as in the NMR structure with a second loop being positioned diagonally across the G-quartets; Chair: all loops being lateral; Mixed: the first and second loops are lateral with the third loop in the propeller orientation
[e]Calculated in HYDROPRO.
[f]Reported X-ray crystal structure optimized by molecular dynamics.
[g]Reported X-ray crystal structure, no molecular dynamics optimization.
[h]Antiparallel NMR structure optimized by molecular dynamics with K^+ ions.
[i]Antiparallel NMR structure with K^+ ions in Na+ positions with minimization but no molecular dynamics optimization.

geometry of a type not previously reported. The most energetically stable chair form allows for a T-A-T-A quartet in the first and third loops. However, this structure, while appealing due to the near perfect stacking, is not the most compact structure among those considered. It is possible to generate structures with higher sedimentation values, but these values are universally lowered while undergoing the molecular dynamics treatment.

DISCUSSION

The results of quantitative sedimentation and fluorescence studies show conclusively that the structure of the human telomere quadruplex described by Parkinson *et al*. (23) cannot possibly be the major conformation that is present in K^+ solution. The solution structure is hydrodynamically more compact than the crystal structure, and the structures of the three TTA loops lack the symmetry of the structure observed in the crystalline state. These results suggest that the crystallographic structure may not be the most appropriate model to use for structure-based design efforts, and that other biologically more relevant structures may predominate in solution. Exactly what these structures are cannot yet be specified, but our biophysical studies elucidate specific features that must exist in solution.

It is not uncommon for quadruplex structures derived by crystallography to differ from those determined in solution (31). For example, the *Oxytrichia* telomere repeat sequence $d(G_4T_4G_4)$ was found by crystallography to form a head-to-tail dimer in K^+, with lateral loops on opposite ends of the structure (49). The NMR structure of the same sequence in either K^+ or Na^+, however, is quite different from the crystal structure (50,51). The NMR structures feature an antiparallel dimer with diagonal loops across each end. Another example is the human thrombin binding aptamer, $d(G_2T_2G_2TGTG_2T_2G_2)$. The crystal structure (52,53) of the thrombin bound form differs from the NMR structures of the aptamer alone with respect to the alignment of the loops (54). Quadruplexes evidently can adopt a variety of conformations, and it is possible that crystal packing forces, crowding, or the dehydrating conditions within the crystal might select for a particular conformation that is not the predominant one in solution. This point will be addressed more fully below.

Thus far, attempts to determine the high-resolution structure of the intact, 22 nt ht-quadruplex in K^+ solution by NMR have proven to be unsuccessful, perhaps because of the presence of multiple conformational forms (55). A two-repeat human telomeric sequence, d(TAGGGTTAGGGT), however, was found to form both parallel and antiparallel G-quadruplexes in K^+ solutions (55). The parallel structure was similar to that observed in the crystal, while the antiparallel structure featured two lateral loops on opposite ends of G-quartet stacks. The two structures could coexist and could interconvert in solution. The interconversion was highly dependent on temperature. The exact relevance of this dimeric structure to the intact unimolecular sequence is not entirely clear. The dimer lacks one of the loops and is, therefore, less topologically constrained compared with the intact, full-length sequence.

What is the structure of ht-quadruplex in K^+ solution? Our biophysical studies cannot provide a definitive answer to that question, but can provide molecular characteristics that help define features of that structure. Along with additional constraints provided by other experimental approaches that have been published, features of a plausible structure emerge. Our sedimentation and fluorescence studies indicate that the K^+ form is hydrodynamically more compact than the Na^+ form, yet that loop residues A1 and A7 are more accessible solvent. The solvent accessibility of loop residues A13 and A19 are identical in K^+ and Na^+. Our data, in general, suggest that the conformational change that results from the substitution of K^+ for Na^+ primarily involves an alteration in loop structures. Early studies showed that loop adenine residues were

generally more reactive toward DEPC in K^+ relative to Na^+, but that the pattern of reactivity remained the same, a finding consistent with our fluorescence quenching data that show greater accessibility of residues A1 and A7. Platinum cross-linking studies (27) reported the formation of A1-G10, A13-G22, A1-A13, A7-A19, G4-A19 and A7-G20 platinum chelates in both K^+ and Na^+. Those results suggest that an antiparallel structure is the predominant form in both K^+ and Na^+. ^{125}I radioprobing experiments support the fact that the antiparallel structure predominates in both K^+ and Na^+, but suggested that the change in ion type facilitated a 'basket' to 'chair' transition, where the diagonal loop observed in Na^+ switched to a lateral loop in K^+[29]. Such a transition would alter the orientation of the two lateral loops on the opposite end from a parallel orientation to an antiparallel one. Our fluorescence quenching data are consistent with that proposal. By changing the diagonal loop to a lateral one, residue A1 would be rendered more accessible to solvent (as observed), while A13 would remain less accessible, buried within the lateral loop structure. Alteration of the loop orientation on the opposite end of the molecule would alter the stacking interactions of A7 and A19. A19 evidently remains buried, while A7 becomes more accessible. Single molecule FRET studies (28) indicated that an antiparallel structure was the dominant (but not the sole) conformation in both K^+ and Na^+.

The data collectively suggest that an antiparallel 'chair' form is most likely the predominant conformation in K^+ solutions. Marathias and Bolton (45) found by solution NMR studies that K^+ favored 'chair' structures for sequences with shorter loop lengths. We find by molecular dynamics that the hydrodynamic properties of a variety of chair structures are generally consistent (within ~10%) with measured sedimentation coefficients in K^+ solution, although we have not yet been able to construct a model that matches the experiment exactly, primarily because we do not know what the exact loop structures might be.

Why is the crystal structure different from that in solution? One possibility is that the crowded, dehydrated conditions in the crystal have selected for a particular conformational form. The experiment in Figure 4 is consistent with that hypothesis. Upon addition of a macromolecular crowding agent, polyethylene glycol, there is a distinct transition of the ht-quadruplex to a different conformational form, as judged by circular dichroism. Another possibility is that the conformation observed in the crystal was selected for by a small molecule 'driver'. The crystals were grown in solutions containing 300 mM KCl, 15% polyethylene glycol 400, 1.7 mM DNA and 2.0 mM BRACO 19, 50 mM potassium cacodylate, pH 6.5. BRACO 19 is a trisubstituted acridine derivative designed to be a G-quadruplex selective binding agent. Results from the Hurley laboratory have shown that G-quadruplex-selective small molecules can act as 'drivers' to act as chaperones that facilitate quadruplex folding (56). The Bolton laboratory has shown that porphyrins can catalyze the interconversion of quadruplex structural types, and in particular can drive both basket- and chair-type structures into parallel-stranded quadruplexes (57). Recent results from the Hurley laboratory showed that the G-quadruplex binders telomestatin and diselenosapphyrin can affect the conformation of the telomeric G-quadruplex found in solution (58). Diselenosapphyrin, in particular, was proposed to select for a hydrid conformation that featured two lateral and one external 'propeller' loop. The combination of crowding and the presence of a driver may well have selected for a quadruplex structure in the crystal that would otherwise not be favored in solution.

The above arguments should not be confused with a suggestion that crystal packing forces may have produced an artifactual quadruplex conformation. Crowding effects are distinct from crystal packing forces and are rooted in fundamental solution thermodynamics, specifically excluded volume effects (59). Crystal packing forces are relatively weak (60). Even though the experimentally determined energetic cost of converting the sodium quadruplex form to the potassium form is only ~2.5 kcal/mol (J. Li and J. B. Chaires, manuscript in preparation), we doubt that crystal packing forces alone could drive a major topological conversion. Crystal packing could exert more subtle effects on base orientations within loops. On the other hand, crowding, which we demonstrate as directly possible in Figure 4, could drive a conformational selection by creating conditions that favor compact conformations or associated complexes. Crystal growth conditions included 15% PEG 400, resulting in significant crowding. We note that in the crystal, quadruplexes are in fact present as dimers (23). The solvent accessible surface of the crystallographic quadruplex monomer was calculated to be 4391 $Å^2$, while the surface area of the associated dimer was 6995 $Å^2$ (the average solvent accessible surface area for the reported antiparallel NMR structures is 3797 $Å^2$). The fact that the dimer seen in the crystal has a significantly lower surface area than twice the surface area of the monomer is fully consistent with an association driven by crowding. It is interesting to note that in the crystal structure the dimer can be viewed as the repeating unit and the loops are stabilizing the lattice by stacking with each other and with neighboring quartets. In fact, all of the loops are participating in such stabilization of the crystal lattice. It is also interesting to note that the calculated energy for the crystal structure form ($E = -18\,914$ kJ/mol) is higher (i.e. more unfavorable) than that for the NMR structure with K^+ replacing Na^+ ($E = -19\,057$ kJ/mol).

Upon completion of our experimental studies, we became aware of recent work that provided similar data. The fluorescence properties of 2-AP in human telomeric DNA were investigated (61), but only in sodium solution. 2-AP was substituted at the 7, 13 and 19 positions, as we have done. The order of accessibility to the quencher ascorbic acid was found to be (from least to most accessible): A13 < A19 < A7. That order agrees with our data using acrylamide as a quencher. A longer fluorescence lifetime for A7 (compared with A13 and A19) was observed, consistent with the steady-state intensity measurements shown in Figure 3. Translational diffusion coefficients were measured for human telomeric DNA by photon correlation spectroscopy in both Na^+ and K^+ solutions (62). A value of 1.4×10^{-6} cm^2/s was found regardless of ion type, in good agreement with the values we calculated from *S*- and *M*-values (Table 1). The finding that there is little difference in the measured diffusion coefficient in Na^+ and K^+ solutions supports our contention that the actual form in potassium solution differs from hydrodynamic properties predicted from the crystal structure.

In the initial report of the parallel-stranded 'propeller' structure, it was suggested that its conformation would facilitate stacking of monomeric units into higher-order telomeric

structures at the end of the chromosome (23). Our sedimentation velocity and sedimentation equilibrium data show unambiguously and definitively that monomeric units do not stack or self-associate in K^+ solution, with no >2% of the population present as higher aggregates. We suggest, though, that stacking of the propeller structure may in fact have relevance and utility. The conformation of the human telomeric G-quadruplex is clearly flexible, with an ensemble of conformational forms accessible. These forms respond to environmental conditions. Such responsiveness could provide a switching mechanism that could allow telomeric DNA to respond to changes in its environment throughout the cell cycle. The different conformational forms might participate in different biological functions at different stages in the cell cycle. The parallel-stranded propeller form might, for example, be used to effectively pack telomeric DNA into an inactive, inaccessible form upon chromosome condensation. Other conformational forms might exist over the course of the cell cycle to facilitate telomere replication or other telomere functions. The key concept is that diverse G-quadruplex conformations exist and that all may have biological relevance. The ability to switch between forms is perhaps key to their biology, providing a kind of allosteric regulatory mechanism. Appropriate drug design efforts need to recognize and embrace the conformational diversity.

SUPPLEMENTARY MATERIAL

Supplementary Material is available at NAR Online.

ACKNOWLEDGEMENTS

Supported by National Cancer Institute grant CA35635 (J.B.C). Funding to pay the Open Access publication charges for this article was provided by the James Graham Brown Foundation.

Conflict of interest statement. None declared.

REFERENCES

1. Wright,W.E., Tesmer,V.M., Huffman,K.E., Levene,S.D. and Shay,J.W. (1997) Normal human chromosomes have long G-rich telomeric overhangs at one end. *Genes Dev*., **11**, 2801–2809.
2. Gellert,M., Lipsett,M.N. and Davies,D.R. (1962) Helix formation by guanylic acid. *Proc. Natl Acad. Sci. USA*, **48**, 2013–2018.
3. Hurley,L.H. (2002) DNA and its associated processes as targets for cancer therapy. *Nature Rev. Cancer*, **2**, 188–200.
4. Mergny,J.L. and Helene,C. (1998) G-quadraplex DNA: A target for drug design. *Nature Medicine*, **4**, 1366–1367.
5. Neidle,S. and Read,M.A. (2000) G-quadruplexes as therapeutic targets. *Biopolymers*, **56**, 195–208.
6. Bodnar,A.G., Ouellette,M., Frolkis,M., Holt,S.E., Chiu,C.P., Morin,G.B., Harley,C.B., Shay,J.W., Lichtsteiner,S. and Wright,W.E. (1998) Extension of life-span by introduction of telomerase into normal human cells. *Science*, **279**, 349–352.
7. Harley,C.B. (1991) Telomere loss: mitotic clock or genetic time bomb? *Mutat. Res*., **256**, 271–282.
8. Sun,H., Bennett,R.J. and Maizels,N. (1999) The *Saccharomyces cerevisiae* Sgs1 helicase efficiently unwinds G–G paired DNAs. *Nucleic Acids Res*., **27**, 1978–84.
9. Sun,H., Karow,J.K., Hickson,I.D. and Maizels,N. (1998) The Bloom's syndrome helicase unwinds G4 DNA. *J. Biol. Chem*., **273**, 27587–27592.
10. Grand,C.L., Han,H., Munoz,R.M., Weitman,S., Von Hoff,D.D., Hurley,L.H. and Bearss,D.J. (2002) The cationic porphyrin TMPyP4 down-regulates c-MYC and human telomerase reverse transcriptase expression and inhibits tumor growth *in vivo*. *Mol. Cancer Ther*., **1**, 565–573.
11. Siddiqui-Jain,A., Grand,C.L., Bearss,D.J. and Hurley,L.H. (2002) Direct evidence for a G-quadruplex in a promoter region and its targeting with a small molecule to repress c-MYC transcription. *Proc. Natl Acad. Sci. USA*, **99**, 11593–11598.
12. Simonsson,T., Pecinka,P. and Kubista,M. (1998) DNA tetraplex formation in the control region of c-myc. *Nucleic Acids Res*., **26**, 1167–1172.
13. Huppert,J.L. and Balasubramanian,S. (2005) Prevalence of quadruplexes in the human genome. *Nucleic Acids Res*., **33**, 2908–2916.
14. Todd,A.K., Johnston,M. and Neidle,S. (2005) Highly prevalent putative quadruplex sequence motifs in human DNA. *Nucleic Acids Res*., **33**, 2901–2907.
15. Hurley,L.H. (2001) Secondary DNA structures as molecular targets for cancer therapeutics. *Biochem. Soc. Trans*., **29**, 692–696.
16. Neidle,S. and Thurston,D.E. (2005) Chemical approaches to the discovery and development of cancer therapies. *Nat. Rev. Cancer*, **5**, 285–296.
17. Jenkins,T.C. (2000) Targeting multi-stranded DNA structures. *Curr. Med. Chem*., **7**, 99–115.
18. Neidle,S. and Parkinson,G. (2002) Telomere maintenance as a target for anticancer drug discovery. *Nature Rev. Drug Discov*., **1**, 383–93.
19. Han,H. and Hurley,L.H. (2000) G-quadruplex DNA: a potential target for anti-cancer drug design. *Trends Pharmacol. Sci*., **21**, 136–142.
20. Hurley,L.H., Wheelhouse,R.T., Sun,D., Kerwin,S.M., Salazar,M., Fedoroff,O.Y., Han,F.X., Han,H., Izbicka,E. and Von Hoff,D.D. (2000) G-quadruplexes as targets for drug design. *Pharmacol. Ther*., **85**, 141–158.
21. Raymond,E., Soria,J.C., Izbicka,E., Boussin,F., Hurley,L. and Von Hoff,D.D. (2000) DNA G-quadruplexes, telomere-specific proteins and telomere-associated enzymes as potential targets for new anticancer drugs. *Invest. New Drugs*, **18**, 123–137.
22. Wang,Y. and Patel,D.J. (1993) Solution structure of the human telomeric repeat d[AG3(T2AG3)$_3$] G-tetraplex. *Structure*, **1**, 263–282.
23. Parkinson,G.N., Lee,M.P. and Neidle,S. (2002) Crystal structure of parallel quadruplexes from human telomeric DNA. *Nature*, **417**, 876–880.
24. Ren,J., Qu,X., Trent,J.O. and Chaires,J.B. (2002) Tiny telomere DNA. *Nucleic Acids Res*., **30**, 2307–2315.
25. Haider,S., Parkinson,G.N., Read,M.A. and Neidle,S. (2003) Design and analysis of G4 recognition compounds. In Demeunynck,M., Bailly,C. and Wilson,D.W. (eds), *DNA and RNA Binders*. Wiley-VCH, Weinheim, Vol. 2, pp. 337–359.
26. Balagurumoorthy,P. and Brahmachari,S.K. (1994) Structure and stability of human telomeric sequence. *J. Biol. Chem*., **269**, 21858–21869.
27. Redon,S., Bombard,S., Elizondo-Riojas,M.A. and Chottard,J.C. (2003) Platinum cross-linking of adenines and guanines on the quadruplex structures of the AG3(T2AG3)$_3$ and (T2AG3)4 human telomere sequences in Na^+ and K^+ solutions. *Nucleic Acids Res*., **31**, 1605–1613.
28. Ying,L., Green,J.J., Li,H., Klenerman,D. and Balasubramanian,S. (2003) Studies on the structure and dynamics of the human telomeric G quadruplex by single-molecule fluorescence resonance energy transfer. *Proc. Natl Acad. Sci. USA*, **100**, 14629–14634.
29. He,Y., Neumann,R.D. and Panyutin,I.G. (2004) Intramolecular quadruplex conformation of human telomeric DNA assessed with 125I-radioprobing. *Nucleic Acids Res*., **32**, 5359–5367.
30. Qi,J. and Shafer,R.H. (2005) Covalent ligation studies on the human telomere quadruplex. *Nucleic Acids Res*., **33**, 3185–3192.
31. Keniry,M.A. (2000) Quadruplex structures in nucleic acids. *Biopolymers*, **56**, 123–146.
32. Laue,T. (2001) Biophysical studies by ultracentrifugation. *Curr. Opin. Struct. Biol*., **11**, 579–583.
33. Laue,T.M. and Stafford,W.F.,III (1999) Modern applications of analytical ultracentrifugation. *Annu. Rev. Biophys. Biomol. Struct*., **28**, 75–100.
34. Garcia de la Torre,J. (2001) Hydration from hydrodynamics. General considerations and applications of bead modelling to globular proteins. *Biophys. Chem*., **93**, 159–170.
35. Garcia de la Torre,J., Huertas,M.L. and Carrasco,B. (2000) Calculation of hydrodynamic properties of globular proteins from their atomic-level structure. *Biophys. J*., **78**, 719–730.

36. Fernandes,M.X., Ortega,A., Lopez Martinez,M.C. and Garcia de la Torre,J. (2002) Calculation of hydrodynamic properties of small nucleic acids from their atomic structure. *Nucleic Acids Res.*, **30**, 1782–1788.
37. Jean,J.M. and Hall,K.B. (2002) 2-Aminopurine electronic structure and fluorescence properties in DNA. *Biochemistry*, **41**, 13152–13161.
38. Johnson,N.P., Baase,W.A. and Von Hippel,P.H. (2004) Low-energy circular dichroism of 2-aminopurine dinucleotide as a probe of local conformation of DNA and RNA. *Proc. Natl Acad. Sci. USA*, **101**, 3426–3431.
39. Nordlund,T.M., Xu,D. and Evans,K.O. (1993) Excitation energy transfer in DNA: duplex melting and transfer from normal bases to 2-aminopurine. *Biochemistry*, **32**, 12090–12095.
40. Ward,D.C., Reich,E. and Stryer,L. (1969) Fluorescence studies of nucleotides and polynucleotides. I. Formycin, 2-aminopurine riboside, 2,6-diaminopurine riboside, and their derivatives. *J. Biol. Chem.*, **244**, 1228–1237.
41. Lakowicz,J.R. (1999) *Principles of Fluorescence Spectroscopy*. Plenum Press, New York.
42. Plum,G.E. (2004) Determination of oligonucleotide molar extinction coefficients. In Beaucage,S.L., Bergstrom,D.E., Glick,G.D. and Jones,R.A. (eds.), John Wiley & Sons, Inc., New York, *Current Protocols in Nucleic Acid Chemistry*, pp. 7.3.1–7.3.17.
43. Schuck,P., Perugini,M.A., Gonzales,N.R., Howlett,G.J. and Schubert,D. (2002) Size-distribution analysis of proteins by analytical ultracentrifugation: strategies and application to model systems. *Biophys. J.*, **82**, 1096–1111.
44. Stafford,W.F. and Sherwood,P.J. (2004) Analysis of heterologous interacting systems by sedimentation velocity: curve fitting algorithms for estimation of sedimentation coefficients, equilibrium and kinetic constants. *Biophys. Chem.*, **108**, 231–243.
45. Marathias,V.M. and Bolton,P.H. (1999) Determinants of DNA quadruplex structural type: sequence and potassium binding. *Biochemistry*, **38**, 4355–4364.
46. Mohamadi,F., Richards,N.G., Guida,W.C., Liskamp,R., Lipton,M., Caufield,C., Chang,G., Hendricksen,T. and Still,W.C. (1990) MacroModel—an integrated software system for modeling organic and bioorganic molecules using molecular mechanics. *J. Comput. Chem.*, **11**, 440–455.
47. Hubbard,S.J. and Thornton,J.M. (1993) NACCESS Computer Program. Department of Biochemistry and Molecular Biology, University College, London.
48. Laughlan,G., Murchie,A.I., Norman,D.G., Moore,M.H., Moody,P.C., Lilley,D.M. and Luisi,B. (1994) The high-resolution crystal structure of a parallel-stranded guanine tetraplex. *Science*, **265**, 520–524.
49. Kang,C., Zhang,X., Ratliff,R., Moyzis,R. and Rich,A. (1992) Crystal structure of four-stranded Oxytricha telomeric DNA. *Nature*, **356**, 126–131.
50. Schultze,P., Smith,F.W. and Feigon,J. (1994) Refined solution structure of the dimeric quadruplex formed from the Oxytricha telomeric oligonucleotide d(GGGGTTTTGGGG). *Structure*, **2**, 221–233.
51. Smith,F.W. and Feigon,J. (1993) Strand orientation in the DNA quadruplex formed from the Oxytricha telomere repeat oligonucleotide d(G4T4G4) in solution. *Biochemistry*, **32**, 8682–8692.
52. Padmanabhan,K., Padmanabhan,K.P., Ferrara,J.D., Sadler,J.E. and Tulinsky,A. (1993) The structure of alpha-thrombin inhibited by a 15-mer single-stranded DNA aptamer. *J. Biol. Chem.*, **268**, 17651–17654.
53. Padmanabhan,K. and Tulinsky,A. (1996) An ambiguous structure of a DNA 15-mer thrombin complex. *Acta Crystallogr. D Biol. Crystallogr.*, **52**, 272–282.
54. Kelly,J.A., Feigon,J. and Yeates,T.O. (1996) Reconciliation of the X-ray and NMR structures of the thrombin-binding aptamer d(GGTTGGTGTGGTTGG). *J. Mol. Biol.*, **256**, 417–422.
55. Phan,A.T. and Patel,D.J. (2003) Two-repeat human telomeric d(TAGGGTTAGGGT) sequence forms interconvering parallel and antiparallel G-quadruplexes in solution:distinct topologies, thermodynamic properties and folding/unfolding kinetics. *J. Am. Chem. Soc.*, **125**, 15021–15027.
56. Han,H., Cliff,C.L. and Hurley,L.H. (1999) Accelerated assembly of G-quadruplex structures by a small molecule. *Biochemistry*, **38**, 6981–6986.
57. Arthanari,H. and Bolton,P.H. (1999) Porphyrins can catalyze the interconversion of DNA quadruplex structural types. *Anticancer Drug Des.*, **14**, 317–326.
58. Rezler,E.M., Seenisamy,J., Bashyam,S., Kim,M.Y., White,E., Wilson,W.D. and Hurley,L.H. (2005) Telomestatin and diseleno sapphyrin bind selectively to two different forms of the human telomeric G-quadruplex structure. *J. Am. Chem. Soc.*, **127**, 9439–9447.
59. Minton,A.P. (2001) The influence of macromolecular crowding and macromolecular confinement on biochemical reactions in physiological media. *J. Biol. Chem.*, **276**, 10577–10580.
60. Dickerson,R.E., Goodsell,D.S. and Neidle,S. (1994) 'The tyranny of the lattice'. *Proc. Natl Acad. Sci. USA*, **91**, 3579–3583.
61. Kimura,T., Kawai,K., Fujitsuka,M. and Majima,T. (2004) Fluorescence properties of 2-aminopurine in human telomeric DNA. *Chem. Commun. (Camb)*, 1438–1439.
62. Wlodarczyk,A., Grzybowski,P., Patkowski,A. and Dobek,A. (2005) Effect of ions on the polymorphism, effective charge, and stability of human telomeric DNA. Photon correlation spectroscopy and circular dichroism studies. *J. Physical Chem.*, **B109**, 3594–3605.